

Advancements in Entangled Photon Pairs in 2D Van der Waals Materials for On-chip Quantum Applications

Abdus Salam Sarkar

Department of Physics, Stevens Institute of Technology, Hoboken, NJ, 07030, USA

Center for Quantum Science and Engineering, Stevens Institute of Technology, Hoboken, NJ,
07030, USA

Email: asarkar5@stevens.edu; salam.phys@gmail.com

Abstract

The next generation of technology is rooted in quantum-based advancements. The entangled photon pair sources play a pivotal role in a wide range of advanced quantum applications, including quantum high precision sensors, communication, computing, cryptography and so on. Scalable on-chip quantum photonic devices have the potential to drive game changing developments in this field. This review article highlights recent breakthroughs in the generation of entangled photon pairs in two dimensional (2D) van der Waals (vdW) materials, with a focus on their applicability to quantum technologies and plausible on-chip integration technology. The article begins by discussing the fundamental principles of entangled photon pairs generation. It provides a comprehensive review of the origin and generation of entangled photons in emerging vdW materials, alongside various optical quantum characterization techniques. The review then explores key physical parameters of the quantum states associated with entangled photon pairs. Additionally, it examines concepts related to the realization of paired photon generation at the quantum limit. The final section focuses on the potential for on-chip integrated quantum device applications. Beyond highlighting recent advancements in quantum-based research, the review also outlines current limitations and future prospects aimed at advancing the field.

Key words: 2D materials, vdW crystals, NLO, Quantum optics, Quantum entanglement, Photon-pairs, SPDC, Quantum state, On-chip quantum applications

1. Introduction

Quantum optics-based technology is rapidly advancing, ushering in a new era of technological innovation.^[1-5] In particular, the emerging quantum applications such as secure quantum key distribution,^[6-8] quantum communication,^[9] quantum sensing,^[10] quantum metrology,^[8,11] quantum imaging,^[12] and distributed quantum computing schemes^[13] are actively testing and pushing the boundaries of fundamental quantum mechanics. Entangled photon-pairs (EPP), a fundamental concept in quantum physics are critical sources and can enable the practical implementation of this advanced technology. A wide variety of entangled photon sources (EPS) have been extensively explored,^[14-17] often relying on spontaneous parametric down conversion (SPDC) in the second harmonic nonlinear crystals. The second order nonlinear ($\chi^{(2)}$) process is the core workhouse for generating entangled quantum light states. The second order non-linear process, which typically occurs in a non-centrosymmetric material with ($\chi^{(2)} \neq 0$).^[18-22] Conventionally, bulk crystals such as beta barium borate (BBO), potassium titanyl phosphate (KTP), and lithium niobate (LN) are used for SPDC.^[1,2,21,23] Most recently, micro resonators and on-chip waveguides have been developed using periodically poled lithium niobate (PPLN) and LN microdisks, which show promise as bright SPDC sources. However, these materials typically hold significantly longer light-matter interaction lengths (d) than their coherence lengths (λ_c). As a result, satisfying the phase-matching condition is essential for achieving high efficiency and brightness in SPDC.^[24]

Since the first isolation of graphene, two-dimensional (2D) van der Waals (vdW) materials have been extensively studied for their nonlinear optical properties.^[19,25] These atomically thin layered materials exhibit remarkable characteristics, particularly in terms of light-matter interactions length ($d \ll \lambda_c$) and enhanced nonlinear responses (**Figure 1**). The crystal symmetry

of these materials plays a pivotal role in determining their nonlinear behavior and corresponding coefficients. For instance, graphene and transition metal dichalcogenides (TMDs) typically possess 2H and 3R crystal structures, which are centrosymmetric. In contrast, materials like black phosphorene and certain metal chalcogenides exhibit lower crystal symmetries, such as D_{2h} and C_{2v} , which are non-centrosymmetric. These symmetry features make them highly suitable for nonlinear, on-chip quantum optical applications, offering a promising high performance platform for subwavelength SPDC sources. In contrast, vdW materials with the $C2$ space group are gaining significant attention due to their exceptional SHG, making them excellent sources for SPDC photons.^[18,26–31] The broad spectral response of vdW materials (**Figure 1a**) even at monolayer thickness, makes them ideal candidates for exploring hyperentanglement in the frequency domain. Moreover, these materials are inherently compatible with nanoscale devices and are well suited for integration into nanophotonic on-chip industrial applications.^[32–36] Various 2D vdW materials have exhibited significantly enhanced nonlinear optical responses compared to conventional bulk materials, and demonstrating strong potential as ultrathin sources for SPDC. For example, Guo et al.^[28] introduced vdW niobium oxychloride (NbOCl_2) as a promising candidate for SPDC applications. The favorable susceptibility tensors within the crystal structure play a pivotal role in enabling SPDC and the generation of entangled quantum states. In another study, polarization entangled quantum states were successfully realized using an engineered vdW bilayer with an orthogonal stacking configuration an architecture not accessible in NbOCl_2 crystals.^[27] Additionally, stacked vdW crystals have been shown capable of generating two or more complex quantum states at the nanoscale. A particular notable achievement is the realization of micrometer scale entangled photon pair sources in 3R-stacked TMD crystals,^[23,37] attributed to the structural integrity of the 3R phase.

The second order nonlinear susceptibility $\chi^{(2)}$ of 3R-phase MoS₂ has been measured to exceed 800 pm/V,^[38] which is comparable to or significantly higher than that of widely used nonlinear crystals such as BBO (3.9 pm/V) and KTP (29.2 pm/V).^[39,40] This excellent nonlinearity effect in multilayer 2D vdW stacks are periodically modulated, offering a new degree of control for nonlinear optical engineering.^[41] Nonetheless, rhombohedral boron nitride (r-BN) has emerged as an excellent source of nonlinear optical signals.^[17,42,43] r-BN exhibits broken inversion symmetry along both its armchair and zig-zag directions, enabling strong nonlinear optical activity. Notably, the nonlinear signal strength increases with the number of layers.^[17] Generation of polarization EPPs has been successfully demonstrated in 2D r-BN, with a measured coincidence rate of 120 Hz and a coincidence-to-accidental ratio (CAR) of 200, corresponding to a fidelity of 0.93. A recent study reported an entangled photon pair generation rate as high as 3100 Hz/(mW×mm), achieved on a tunable platform for Bell state generation by varying the pump polarization without compromising entanglement quality. The highest reported fidelity of the polarization entangled state reached an exceptional level, demonstrating the quality and robustness of the generated entanglement. **Figure 1e** presents the timeline of the discovery of 2D van der Waals materials and the generation of photon pairs.

In parallel, other quasiparticle phenomena beyond entangled photon pairs are actively being explored in 2D vdW materials. These include electron-hole pairs (e-h),^[44] excitons,^[45-47] magnetic excitons (m-e),^[48] magnon-magnon interactions,^[49-51] and magnon-photon-phonon coupling,^[52] chiral phonons,^[53,54] electron-phonon (e-p) interactions,^[55] single-photon sources and chiral phonon dynamics,^[14] as well as valley physics,^[47,56-58] and anti-parity-time (a-p-t) symmetry phenomena,^[59] are also gaining momentum. Despite this broad progress, the generation of entangled photon pairs in vdW materials stands out as a key advancement for next-generation, on-

chip integrated quantum technologies. This is due to the inherently rich nonlinear quantum optical properties enabled by these layered vdW materials.

This review presents the latest developments in the generation of quantum-entangled photon pairs in emerging vdW materials. The underlying physical mechanisms of entanglement via SPDC and the associated nonlinear optical properties are highlighted. Special attention is given to the influence of crystallographic structure on nonlinear quantum processes and its critical role in enabling SPDC. The realization of entangled quantum states in vdW materials is also discussed, including quantum state tomography, as well as the evaluation of state quality and purity for integrated on-chip quantum applications. In addition to demonstrating the potential and significance of EPP generation in vdW systems, this article outlines current limitations and explores emerging opportunities and future prospects in the field.

2. Nonlinear optics crystallography and entanglement photon pairs generation

Current methods for generating EPPs include parametric amplification,^[31] four-wave mixing,^[60] and SPDC across various platforms.^[61] The nonlinear crystals and quantum dots have emerged as key materials at the forefront of this research. In these material systems, nonlinear optical effects play a pivotal role in the generation of entangled photon pairs. In particular, the crystallographic structure of a material is fundamental to the emergence of nonlinear effects. Nonlinear optical effects arise when the material's polarization (P) no longer responds linearly to an applied electric field (E). Specifically, the polarization is described by the following expansion:

$$P(t) = \epsilon_0 \chi^{(1)} E(t) + \epsilon_0 \chi^{(2)} E^2(t) + \epsilon_0 \chi^{(3)} E^3(t) + \dots + \epsilon_0 \chi^{(n)} E^n(t) \quad (1)$$

where, ϵ_0 denotes the vacuum permittivity, $\chi^{(1)}$ is the linear (first order) susceptibility, and $\chi^{(n)}$ represents the n th-order nonlinear susceptibility of the material for $n>1$. Equation 1 can be expressed in the frequency domain, where $\chi^{(n)}(\omega)$ denotes the n th order nonlinear susceptibility at frequency ω .

Nonlinear optical processes are generally classified as either parametric or nonparametric. In a parametric process, energy exchange occurs exclusively among interacting photons, and the total photon energy is conserved. In this case, the real part of the susceptibility χ is relevant. Additionally, both linear and angular momentum of the optical fields remain unchanged between the initial and final states. Since the quantum state of the material remains unaltered, the process occurs on an extremely short time scale governed by the energy-time uncertainty principle, ($\Delta t=\hbar/2\Delta E$). Such processes are responsible for frequency conversion phenomena. A prime example is second harmonic generation (SHG), where frequency doubling occurs through a virtual intermediate state. On the other hand, nonparametric processes involve energy exchange between photons and the material itself. In these processes, the imaginary component of the susceptibility χ becomes significant (i.e., non-zero). The physical mechanism entails real energy transfer between the initial and final states of the system. Because this energy exchange involves transitions between real quantum states, nonparametric processes typically occur on longer timescales compared to parametric processes. Examples of such processes include two-photon absorption, saturable absorption (SA), and stimulated Raman scattering (SRS).

Here, primary focus on second-order nonlinearity and the influence of crystallographic effects on this process. In **Equation 1**, the polarization P includes a term proportional to E^2 , indicating that second-order nonlinear effects arise when the induced polarization is proportional to the square of the applied electric field ($P \propto E^2$). The second-order susceptibility, $\chi^{(2)}$, plays a

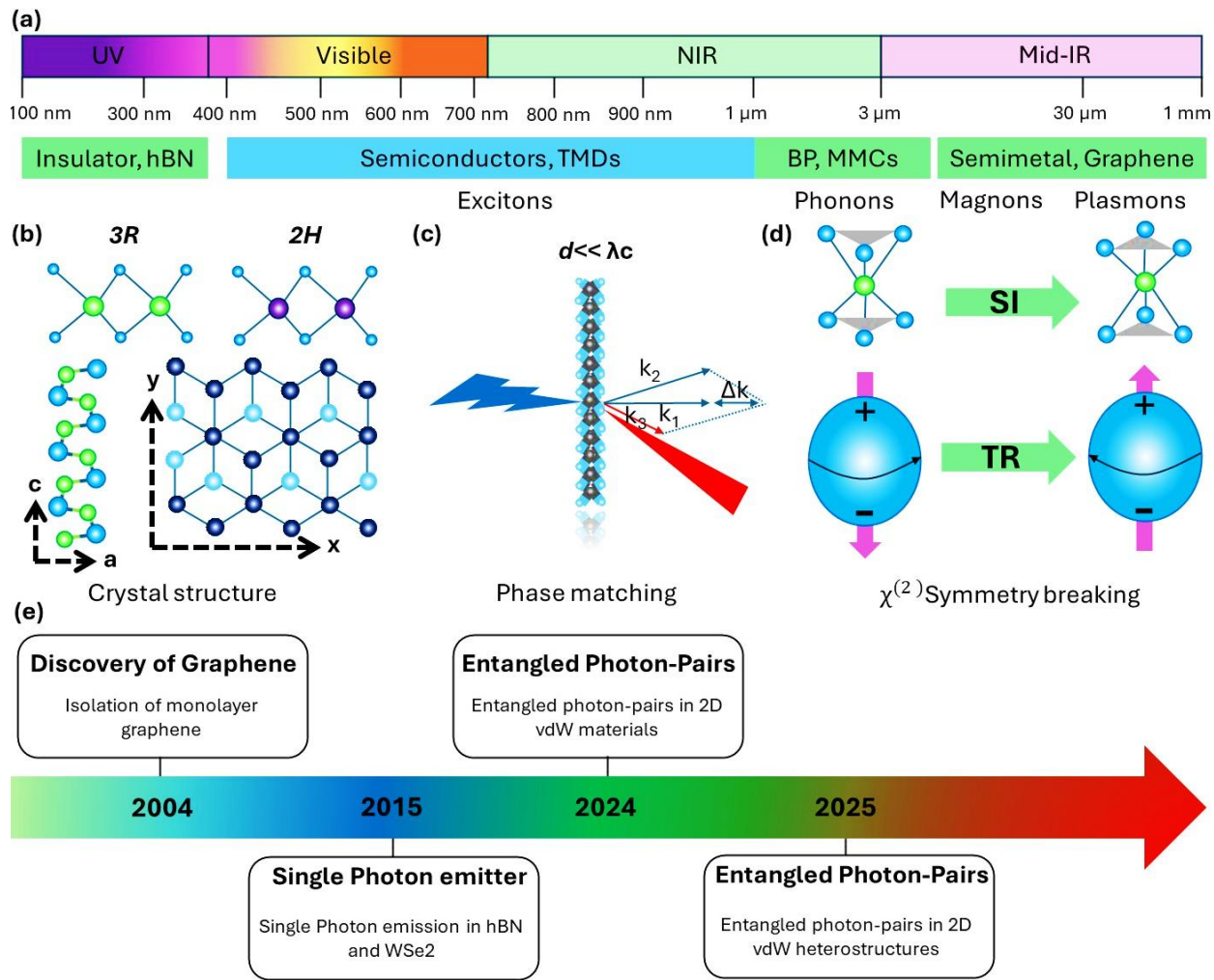


Figure 1| Key features of atomically thin layered materials for nonlinear optics and quantum entanglement. **a**, The electromagnetic spectrum and the unique optical properties of 2D materials across a broad spectral range. Distinct optical features arise from excitations such as excitons, phonons, plasmon and magnons. **b**, Crystal structures of layered materials. *Top*: Different symmetries of an atomically thin 2D TMD of MoS₂, including hexagonal (2H) and rhombohedral (3R) phases. *Bottom left*: Crystal structure of an anisotropic atomically thin monochalcogenide (MX), where blue atoms represent M (metal) and green atoms represent X (chalcogen). The *a* and *c* directions denote the armchair and zigzag directions, respectively. *Bottom right*: Crystal structure of rhombohedral boron nitride (r-BN), with *x* and *y* representing the armchair and zigzag directions.

of the crystal. **c**, Schematic illustrating the impact of short propagation lengths ($d \ll \lambda_c$) on phase-matching conditions. k_1 and k_2 are wave vectors of two photons and $\Delta k = k_2 - 2k_1$. **d**, Symmetry breaking in atomically thin crystals, involving both spatial (SI) inversion and time-reversal (TR) symmetry and **e** A historical timeline of 2D van der Waals materials and the development of entangled photon pair generation.^[62–65]

major role in these nonlinear optical processes. In particular, $\chi^{(2)}$ is essential for SHG in crystalline materials. SHG is only permitted in materials that lack inversion symmetry i.e., those with a non-centrosymmetric crystal structure. In centrosymmetric materials, $\chi^{(2)}$ vanishes, making second-order nonlinear processes such as SHG forbidden. Since the second-order nonlinear processes require broken inversion symmetry in the crystal, understanding symmetry is essential. **Figure 1d** illustrates the symmetry breaking present in various crystals, including both spatial inversion (SI) symmetry and time-reversal (TR) symmetry. A wide range of materials has been studied to explore how symmetry influences nonlinear optical processes such as SHG.^[18,19,66] For example, TMDs exhibit layer number dependent SHG ($I_{\text{SHG}} \propto N^2$).^[22,67] In the 2H phase, odd numbered layers break inversion symmetry and therefore support SHG. In contrast, even numbered layers restore inversion symmetry, resulting in the disappearance of SHG. In the case of the 3R phase (rhombohedral stacking), the crystal structure inherently lacks inversion symmetry, making it non-centrosymmetric. As a result, 3R-phase TMDs exhibit non-zero SHG, regardless of the number of layers.

Materials with a puckered or wavy lattice structure exhibit reduced crystal symmetry such as the (D_{2h}) point group compared to conventional 2D materials like graphene (D_{6h}) and TMD.

This reduction in symmetry leads to more intriguing nonlinear optical phenomena. The lower symmetry of these crystals results in broken inversion symmetry and introduces in-plane anisotropy. Additionally, the buckled structure gives rise to direction dependent optical properties, making these materials particularly promising for polarization sensitive and anisotropic nonlinear optical applications. Most recent development of monolayer 2D monochalcogenides (MMCs) have been shown to exhibit low crystal symmetry belonging to the C_{2v} point group, with an orthorhombic crystal structure (Pnma space group).^[68–71] In this structure, inversion symmetry is further broken, enhancing their nonlinear optical response. This unique crystallographic feature gives rise to novel optical polarization properties, enabling the observation of new orders of optical nonlinearity and anisotropy.^[71–75]

On another note, 2D magnetic materials have also exhibited SHG,^[20,76–82] which classified into two types: *c*-type and *i*-type.^[83,84] Among these, *c*-type materials have been more widely reported to show SHG, primarily due to their non-centrosymmetric antiferromagnetic (AFM) nature. Interestingly, even centrosymmetric AFM materials have demonstrated giant SHG responses, attributed to their magnetic structures, which break both spatial inversion (SI) and time-reversal (TR) symmetries.^[77]

2.1 Quantifying Nonlinear Coefficients and Conversion Efficiency

The nonlinear coefficient and conversion efficiency are key metrics for evaluating the performance of nonlinear optical materials.^[40] In atomically thin layered materials, values of $\chi^{(2)}$ have been reported in the order of nanometers per volt (nm/V), which is significantly higher than those observed in conventional nonlinear crystals, where $\chi^{(2)}$ is typically on the order of picometers per

Table 1. The second order nonlinear coefficient for the vdW materials. ME is mechanical exfoliation, LPE is liquid phase exfoliation, CVT is chemical vapor transport, PVD is physical vapor deposition, VLSS is vapor-liquid-solid synthesis method and MSAA is metal solvent assisted approaches.

Materials	Prep	Substrate	Layer number	SHG	$\chi^{(2)}$	Ref
	Method			Wavelength		reference
				(nm)		es
MoS₂	ME	SiO ₂	Single layer	405	10000 pm/V	[85]
	CVD	SiO ₂	Single layer	405	5000 pm/V	[85]
	ME	SiO ₂	Single layer	950	800 pm/V	[38]
MoSe₂	ME	Si	Single layer	775	7800 pm/V	[86]
		waveguide				
	CVD	SiO ₂	Single layer	810	50 pm/V	[87]
WS₂	ME	SiO ₂	Single layer	416	4500 pm/V	[88]
WSe₂	ME	SiO ₂	Single layer	408	5000 pm/V	[89]
h-BN	ME	Fused Silica	Multilayer (36.2 nm)	406	42 pm/V	[90]
		Quartz	Few layer	405	200×10^{-11} m/V	[66]
	CVD	Sapphire	Single layer	1046	83.2 pm/V	[91]
r-BN	VLSS	fused silica	730 nm	800	30 pm/V	[43]
SnS	PVD	Mica	Multilayers (7 nm)	800	100 pm/V	[75]

NbSe₂	ME	Quartz	1L	1030	1.0×10^3 pm/V	[92]
			3L		~ 73 pm/V	
NbOCl₂	CVD	-	Single Crystal	532	160 pm/V	[27]
NbOBr₂	CVT	Si	10 nm	1500	9.16×10^{-11} m/V	[18]
NbOI₂	CVT	Quartz	multilayer	425-525	10^{-9} m/V	[93]
Perovskite	Chemical	-	-	850	0.68 pm/V	[94]
MOF	Chemical synthesis	Quartz	12.2 μ m	1030	~ 19.86 pm/V	[95]

volt (pm/V). In particular, Group IV monochalcogenides have demonstrated remarkably high $\chi^{(2)}$ values. However, these values vary widely among layered materials due to several influencing factors, including material quality, fabrication methods, strain, stress, and doping levels. The intensity of SHG, $I_{2\omega}$, is estimated by:

$$I_{2\omega} \propto I_0^2 l^2 \text{sinc}^2 \left(\frac{\Delta k \cdot l}{2} \right) \quad (2)$$

where I_0 is the input intensity, l is the propagation length, and Δk is the phase mismatch. Ideally, efficient frequency conversion requires $\Delta k=0$. For example, the estimated $I_{2\omega}$ of monolayer MoS₂ at 800 nm is approximately 10^{-7} , while WSe₂ exhibits a lower value on the order of 10^{-10} . Notably, SnS and SnSe have demonstrated extraordinarily high SHG intensities, with the highest $I_{2\omega}$ values estimated to be for SnS and SnSe, respectively. The key parameters, including $\chi^{(2)}$, for various emerging layered materials are summarized in **Table 1**.

2.2 Spontaneous parametric down conversion (SPDC)

Spontaneous parametric down-conversion (SPDC) is a nonlinear optical process, also known as a form of difference frequency generation (DFG).^[61,96] In this process, a high energy pump photon spontaneously decays into two lower energy photons, referred to as the signal and idler photons (**Figure 2a**). This process conserves both energy ($\omega_1 = \omega_2 + \omega_3$; 1 and 2 correspond to *signal* and *idler*) and momentum ($k_1 = k_2 + k_3$; 1 and 2 correspond to *signal* and *idler*) (**Figure 2a**). The signal and idler photons are always produced as a pair, and they can become entangled in various degrees of freedom such as polarization, energy-time, or position-time. When the signal and idler photons have orthogonal polarizations, the system can form a polarization entangled Bell state, which is characteristic of Type-II SPDC. Therefore, SPDC serves as a fundamental mechanism for generating entangled photon pairs and plays a vital role in many quantum optics and quantum information experiments. Moreover, the ultrathin vdW materials offer great potential as optically enabled sources of entangled photons through SPDC.

3. Entanglement in 2D vdw materials

Entangled photon pairs are a fundamental concept in quantum physics, particularly in quantum optics and quantum information science. When two photons are entangled, they exhibit correlations in their physical properties such as polarization, momentum, energy, parity, spin that are stronger than what is possible under classical physics, even when separated by large distances. This phenomenon is a direct consequence of quantum entanglement, a nonclassical link between particles that was famously discussed in the Einstein-Podolsky-Rosen (EPR) paradox.

Entangled photon pairs in vdW materials represent a frontier in quantum photonics, where 2D layered crystals such as TMDs, niobium oxide dihalides NbOX_2 (X = Cl, Br, I) enable compact

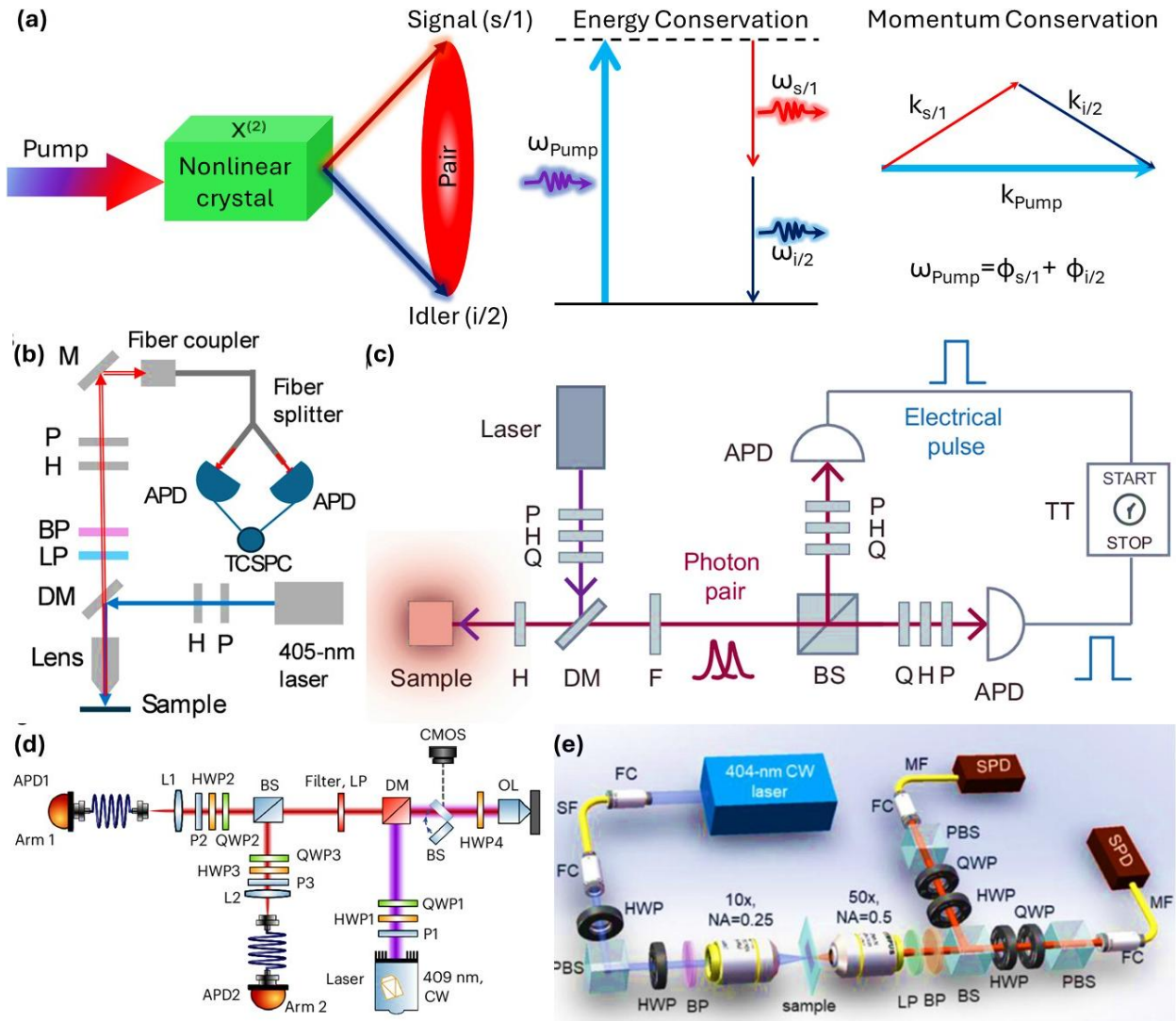


Figure 2| Fundamentals and experimental setup for generating quantum-entangled photon pairs. **a** Schematic illustration of the spontaneous parametric down-conversion (SPDC) process. A pump beam from a laser source interacts with a nonlinear crystal, producing pairs of photons known as the signal (s or 1) and idler (i or 2). The process adheres to the conservation laws of energy and momentum within the nonlinear medium. Energy conservation is expressed as $\omega_{\text{Pump}} = \phi_{s \text{ or } 1} + \phi_{i \text{ or } 2}$ where 1 and 2 denote the signal and idler photons, respectively. **b**, Optical setup for SPDC photon pair generation, adapted from Liang *et al.*^[17] A 405 nm continuous wave

(CW) laser serves as the pump source. The nonlinear optical (NLO) signal generated via SPDC passes through a dichroic mirror and optical filters, then is coupled into a fiber splitter. The split signals are detected by two avalanche photodiodes (APDs). Time correlated single photon counting (TCSPC) is employed to analyze the signals from the APDs. Reproduced with permission.^[17] Copyright 2025, AAAS. **c**, Optical setup used for SPDC characterization by Lyu et al. A continuous wave (CW) laser is employed as the pump source. The setup includes polarizers, a dichroic mirror (DM), and a beam splitter (BS). The generated signal and idler photons are coupled into optical fibers, detected by avalanche photodiodes (APDs), and analyzed using a time tagger (TT). Reproduced with permission.^[97] Copyright Creative Commons CC-BY-NC-ND 2025, Nature Springer Ltd. **d**, Hanbury Brown-Twiss (HBT) setup used to characterize the entangled photon pairs. This configuration enables measurement of photon correlations and coincidence detection. Reproduced with permission.^[65] Copyright 2025, Nature Springer Ltd. and **e**, Schematic illustration of the optical setup used for polarization quantum state tomography. Adopted from Gao et al.^[23] Copyright Creative Commons CC-BY-NC-ND 2024, Nature Springer Ltd.

and tunable quantum light sources. These materials exhibit strong nonlinear optical effects, excitonic effects and spin valley coupling, which can be harnessed to generate polarization entangled photon pairs through processes such as biexciton exciton cascades. The atomically thin nature and high optical quality of vdW heterostructures allow for precise control over light matter interactions, phase matching and their integration into photonic platforms makes them promise for on-chip quantum technologies.^[98] Additionally, the tunability of band alignment and excitonic properties via stacking angle, strain, or dielectric environment enhances the potential as scalable sources for quantum communication and quantum information processing.

3.1. Experimental setup to generate Entangled photon pairs

Entangled photon pair generation is typically realized using the SPDC techniques. The experimental setup is designed to produce customized entangled photon pairs. In the basic configuration, a laser source is used to excite a nonlinear material. The pump beam first passes through a polarizer and a half wave plate, followed by a dichroic mirror. The resulting photoexcited signal is filtered and then split into two paths. Each of these split beams passes through a combination of quarter wave plates, half wave plates, and polarizers. The signals are then collected at two ends using avalanche photodiodes (APDs). To analyze the SPDC signal, coincidence measurements are carried out using a time tagger or time correlated single photon counting (TCSPC) system. For instance, Liang et al.^[17] utilized a fiber coupled collection setup. In their work, a continuous wave (CW) laser at 405 nm was used to excite an 2D r-BN sample. The emitted signal photons passed through a sequence of filters, mirrors, and polarizers (**Figure 2b**), before being coupled into an optical fiber via a fiber beam splitter. The split photons were then detected by APDs, and coincidence measurements were conducted using a TCSPC system.

On the other hand, a free space optical setup can be employed to collect SPDC photon pairs and perform coincidence measurements (**Figure 2d**). The photoexcited SPDC photon pairs are filtered and transmitted through a series of polarization optics. Instead of using a fiber coupled beam splitter, the photon pairs are separated into two paths using a free space beam splitter. A similar optical configuration has been demonstrated by Kallioniemi et al.^[65] In all these setups, the generated SPDC photon pairs are collected in reflection mode.

Qiu and co-workers^[23] have presented the SPDC optical setup from multiple perspectives (**Figure 2e**). In their configuration, SPDC photon pairs are generated and collected in transmission mode from a nonlinear sample. Specifically, the nonlinear material is placed on a transparent

PDMS substrate to facilitate signal acquisition. The generated SPDC photons are collected using an objective lens and subsequently split into two distinct paths. These split photons pass through quarter- and/or half wave plates and a polarizing beam splitter (PBS), before being coupled into multimode fibers. Finally, the signal and idler photons are detected by two single photon detectors. The coincidence rate of the entangled photon pairs is measured using a TCSPC module.

Determining the total photon pair detection efficiency, η_{tot} , is a key measure of the overall performance of the setup. Specifically, η_{tot} is calculated as the product of individual contributing factors^[64] $\eta_{tot} = T_{opt}^2 \times T_{coupl}^2 \times \eta_{BS} \times \eta_{detec}^2 \times \eta_{LP}^2$. Here, T_{opt} is the single photon optical transmission, accounting for losses from filters, mirrors, lenses, etc.; T_{coupl} is the fiber coupling efficiency; η_{BS} represents the non-uniformity and probabilistic splitting of the (fiber or nonfiber) beamsplitter; η_{detec} is the detection efficiency of the detectors at the degenerate SPDC wavelength, averaged over different polarizations; and η_{LP} is the spectral detection factor associated with the long pass filter. The η_{tot} for photon pairs generated in TMDs is approximately 0.6%.

3.2. Entanglement in 2D vdW materials & heterostructures

The generation of entangled photon pairs in 2D rhombohedral phase boron nitride (r-BN) has garnered significant attention due to its unique symmetrical properties (**Figure 3a**). Unlike conventional hexagonal boron nitride, which exhibits a centrosymmetric crystal structure in even numbered layers thereby suppressing second-order nonlinear optical processes r-hBN intrinsically breaks inversion symmetry owing to its ABC-type interlayer stacking sequence. This broken symmetry is critical for enabling efficient second-order nonlinear processes, such as SHG, which

are essential for quantum photonic applications including entangled photon pair production. The diminished nonlinear response in centrosymmetric hBN structures leads to a significantly reduced entanglement signal. In contrast, r-BN's non-centrosymmetric stacking facilitates stronger nonlinear interactions, thereby enhancing entangled photon generation efficiency. Gao and co-workers^[97] have experimentally demonstrated the tunability of EPPs emission in 2D r-BN, a vdW insulating material. The quantum state of the generated entangled photon pairs actively controlled by manipulating the polarization orientation of the incident pump field. In this context, hexagonal 2D r-BN is investigated under a polarized optical pump field. The resulting second-order nonlinear polarization response in the material is described by the relation:

$$P_{\alpha}^{2\omega} = \varepsilon_0 \chi_{\alpha\beta\gamma}^{(2)} E_{\beta}^{\omega} E_{\gamma}^{\omega} \quad (3)$$

where ε_0 is the free space permittivity, $\chi_{\alpha\beta\gamma}^{(2)}$ is the second order nonlinear susceptibility (SONS) and α, β, γ is x or y is the coordinates, E_{β}^{ω} and E_{γ}^{ω} are the components of the electric field of the pump at frequency of ω . In a monolayer hBN the nonvanishing SONS is $\chi_{yyy}^{(2)} = -\chi_{yxx}^{(2)} = -\chi_{xxy}^{(2)} = -\chi_{xyx}^{(2)} = |\chi^{(2)}|$, where x and y corresponding to the armchair and zig-zag direction of the crystal.

The six-fold symmetry observed in the SPDC signal response exhibits periodic maxima and minima as a function of the pump polarization angle. Under co-polarized detection conditions, the SPDC signal reaches a maximum when the pump polarization is aligned along the armchair direction of the r-BN crystal, and a minimum when aligned with the zigzag direction (**Figure 3b**). This behavior is the dominance of the nonzero tensor component $\chi_{yyy}^{(2)}$ in second-order nonlinear susceptibility, as indicated in **equation 3**. The six-fold symmetry remains preserved under cross-polarized pump excitation, except for a phase shift of 30° , which is a symmetry rotation due to

tensorial selection rules. Notably, when the pump field is aligned along the zigzag direction under cross-polarized conditions, the photon pair generation is enhanced, corresponding to the contribution from the non-zero component $\chi_{xyx}^{(2)}$. In a complementary configuration, the analyzer is rotated while the pump polarization is held fixed (**Figure 3d-f**). The resulting two-lobed symmetry patterns can be interpreted based on the quantum state probability amplitude

$$\Phi = \frac{\cos(\varphi_p)}{\sqrt{2}} (|HV\rangle + |VH\rangle) + \frac{\sin(\varphi_p)}{\sqrt{2}} (|HH\rangle - |VV\rangle) \quad (4)$$

where φ_p denotes the pump polarization angle. When the analyzer is set at an angle θ , the resulting quantum states exhibit characteristic angular dependencies. The coincidence count rate follows the analyzer angle, exhibiting modulation proportional to $\sin^2(\varphi_p + 2\theta)$, $\sin^2\varphi_p$, or zero, depending on the specific analyzer pump angle configuration. These angular dependencies reflect the underlying polarization entanglement and the anisotropic nonlinear optical response of the r-BN crystal. The rotational dependence of the pump polarization allows for tunable modulation of the EPPs characteristics, making r-hBN a promising platform for polarization engineered quantum light sources.

On another report the entangled photon pairs that are generated in r-BN for the on chip integrated quantum applications is reported. The polarization analysis of generated photon pairs is explained with crystal symmetry. The system is defined with special polarization relationship between the pump, signal and idler light is

$$|R\rangle_p \xrightarrow{\text{SPDC}} |L\rangle_s |L\rangle_i \quad (5a)$$

$$|L\rangle_p \xrightarrow{\text{SPDC}} |R\rangle_s |R\rangle_i \quad (5b)$$

$$|H\rangle_p \xrightarrow{\text{SPDC}} \frac{1}{\sqrt{2}} (|H\rangle_s |H\rangle_i - |V\rangle_s |V\rangle_i) \quad (6a)$$

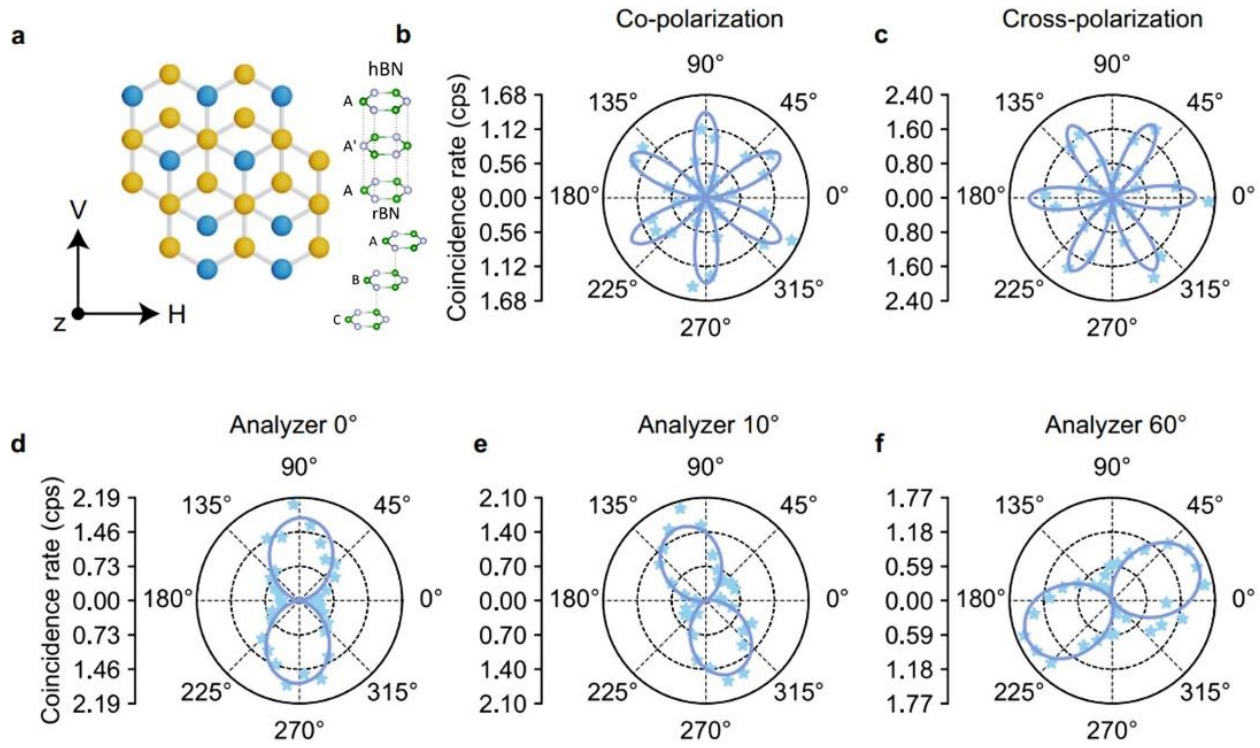


Figure 3| Quantum entangled photon pairs from a van der Waals insulator.

a, *Left:* Schematic of the r-BN crystal structure. *Right:* Comparison of the crystal structures and stacking sequences of h-BN and r-BN. The armchair (V) and zig-zag (H) directions of the crystal are indicated. **b,** Coincidence count rate as a function of incident pump polarization in the co-polarization configuration, where the polarization of both collection arms is aligned parallel to the incident pump polarization. **c,** Coincidence count rate in the cross-polarization configuration, where one collection arm is aligned parallel and the other perpendicular to the incident pump polarization. **d-f,** Pump polarization dependent coincidence rates with fixed analyzer angles in the collection arms. Adapted from.^[97] Copyright 2025, Springer Nature.

where R and L are represented the horizontal (H) and vertical (V) polarization basis. The above equation of the polarization evolution process of SPDC becomes

$$|V\rangle_p \xrightarrow{\text{SPDC}} \frac{-1}{\sqrt{2}} (|H\rangle_s |V\rangle_i - |V\rangle_s |H\rangle_i) \quad (6b)$$

When the pump is arbitrarily linear polarized then the SPDC is projected as a

$$\frac{-\cos\varphi_p}{\sqrt{2}} (|H\rangle_s |V\rangle_i - |V\rangle_s |H\rangle_i) + \frac{-\sin\varphi_p}{\sqrt{2}} (|H\rangle_s |H\rangle_i - |V\rangle_s |V\rangle_i) \quad (7)$$

where φ_p is the angle between the pump and the V polarization direction. A constant SPDC coincidence rate is observed as varied pump polarization, even in the absence of a polarizer at the detector (**Figure 4a**). In contrast, distinct six-fold symmetric patterns emerge when both the pump

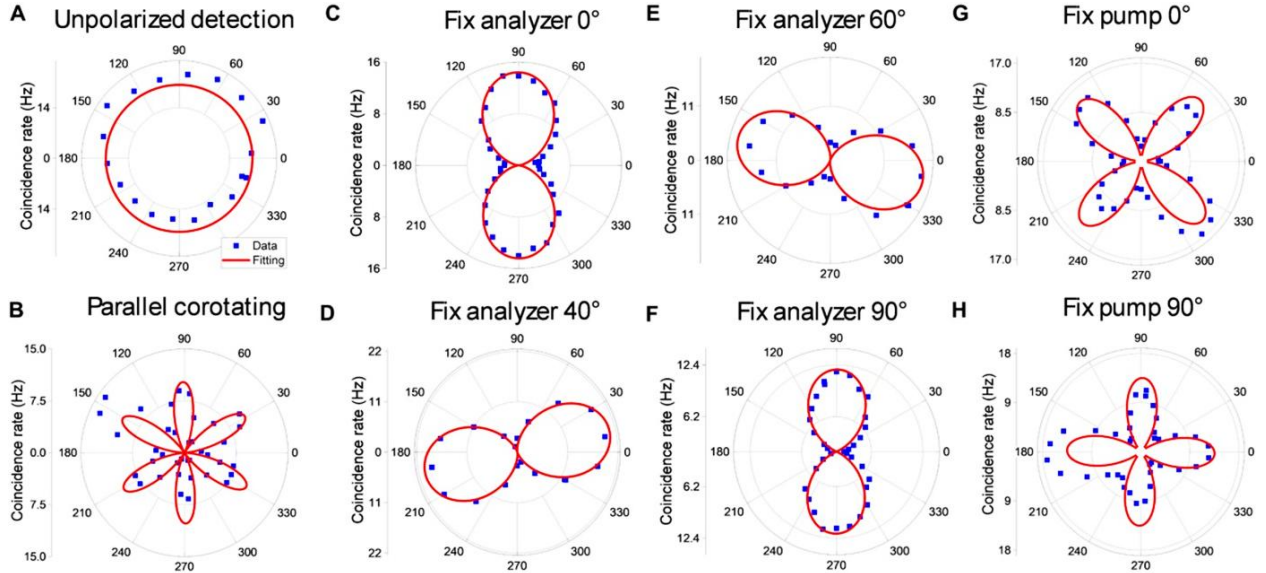


Figure 4 | Photon pair generation and polarization analysis in r-BN. **a**, Coincidence count rate as a function of pump polarization angle (φ_p), measured without any polarization filters at the detectors. **b**, Coincidence rate when both the pump and detector polarizations are rotated simultaneously ($\varphi_p = \varphi_{pol}$). The dependence follows $R_{\text{SPDC}} \propto \sin^2(3\varphi_p)$. **c-f**, Coincidence rates as a function of φ_p with fixed analyzer (detector) polarization angles φ_{pol} set at 0° , 40° , 60° , and

90°, respectively. The dependence follows $R_{SPDC} \propto \sin^2(2\varphi_{pol} + \varphi_p)$. **g, h**, Coincidence rates with fixed φ_p at 0° and 90°, respectively, as the analyzer polarization angle φ_{pol} is varied. The dependence behavior is described by the relation $R_{SPDC} \propto \sin^2(2\varphi_{pol} + \varphi_p)$. Reproduced from Liang *et al.*,^[17] Copyright 2025, AAAS.

and analyzer polarizations are kept parallel and rotated simultaneously (**Figure 4b**). The observed maxima and minima in the SPDC coincidence rate correspond to the armchair and zig-zag directions of the crystal plane, respectively, indicating that the crystal orientation plays a crucial role in determining the coincidence generation rate.

When the analyzer is aligned along the zig-zag direction (0°) and the pump polarization is set along the armchair direction, the coincidence rate follows a $\sin^2 \varphi_p$, dependence (**Figure 4c**). Furthermore, the polarization dependent coincidence rate shown in **Figures 4c-f** exhibits a dependence proportional to $\sin^2(\varphi_p + 2\varphi_{pol})$. By fixing the pump polarization and rotating the analyzer angle, the coincidence rate varies as $\sin^2(2\varphi_{pol} + \varphi_p)$, as demonstrated in Figures G and H.

Beyond BN, the two-crystal geometry approach is employed to generate entangled photon pairs.^[65] In this method, two perpendicular vdW crystals of 2D niobium oxide dichloride (NbOCl_2) are used (**Figure 5a**). Entangled photon pairs are generated via SPDC occurring in either of the two crystals. The indistinguishability of the down conversion process between the two orientations leads to the creation of an entangled photon pair is

$$|\emptyset^+\rangle = |H\rangle|H\rangle + |V\rangle|V\rangle \quad (8)$$

The states $|H\rangle|H\rangle$ and $|V\rangle|V\rangle$ correspond to photon pairs generated along the optical axes of the first and second crystals, producing horizontally and vertically polarized photon pairs, respectively. In this system, coincidence count depends on the pump polarization and exhibits strong directional dependence. Specifically, the peak coincidence counts for one flake occurs when the pump polarization is perpendicular to that of the other flake (**Figure 5b, c**). Furthermore, a remarkably high nonlinear coefficient has been achieved, along with polarization dependent enhancements in the coincidence rates.

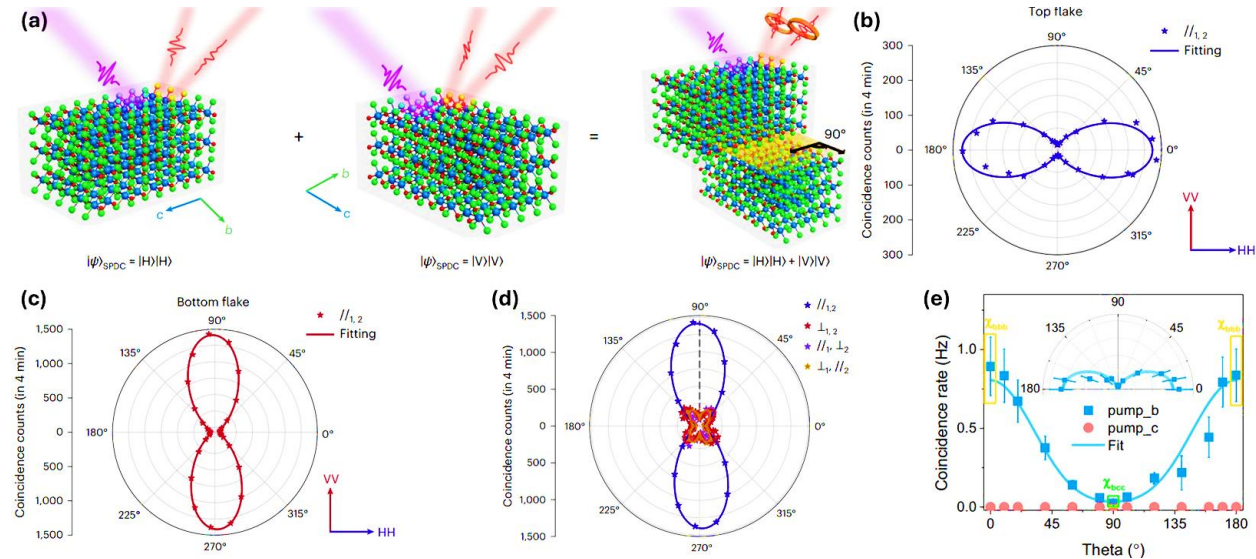


Figure 5 | Entangled Photon Pair Generation in NbOCl₂. **a**, Conceptual illustration of entangled photon pair generation using a two-crystal geometry in NbOCl₂, a 2D vdW material. **b, c**, Pump polarization dependent coincidence rates measured from the top and bottom layers of the crystal, respectively. **d**, All polarization mode pump polarization dependent coincidence. The ‘//’ and ‘ \perp ’ sign denotes the co-polarized and cross-polarized to the pump beam in the corresponding collection arms 1 and 2, respectively. Reproduced with permission from.^[65] Copyright 2024, Springer Nature. **e**, Polarization dependent photon pair coincidence rate in NbOCl₂ with error bars.

The inset shows the corresponding polar coordinate plot. Adapted from.^[23] Copyright 2024, Springer Nature.

4. Quantum state tomography and applications

Quantum state tomography is used to measure the generated polarization quantum state and to demonstrate entanglement between the signal and idler photons.^[23,65,99–102] Various optical components are typically used to deterministically separate entangled photon pairs. A series of waveplates and polarizers in the detection path allows for the setting of arbitrary and independent polarization bases. For example, the density matrix $\hat{\rho}$ of the polarization quantum state can be fully determined by performing projections onto 16 different basis states.^[103] In some cases, an established maximum likelihood method is employed to determine a physically valid density matrix $\hat{\rho}$. The real and imaginary components of the density matrix are extracted from various vdW materials, as shown in **Figure 6**. For instance, Kallioniemi et al.^[65] reconstructed a density matrix that closely resembles the expected quantum state (**Figure 6a**). The results demonstrate a fidelity of $86 \pm 0.7\%$, indicating a high level of quantum state engineering. Concurrently, concurrence C is a measure of photon state entanglement, with values ranging from 0 to 1. Specifically, $C=0$ corresponds to a completely separable (non-entangled) state, whereas $C=1$ indicates a maximally entangled state.^[104,105] For the NbOCl_2 system, the estimated concurrence is 0.87 ± 0.010 . In another report, the polarization state of photon pairs generated in a single layer (1L) NbOCl_2 crystal was investigated.^[23] Notably, the polarization of the generated photon pairs is independent of the pump polarization and followed an HH state, where H denotes polarization along the b -axis of the crystal (**Figure 6b**). These HH-state photon pairs exhibited a high fidelity of 0.95 ± 0.02 . Importantly, the generation of photon pairs in the 1L crystal is constrained by the crystal's symmetry, which is inherently polarization independent. As a result, the system does not exhibit polarization

entanglement. This observation directly correlates with the structure of the crystal's nonlinear susceptibility tensor. The nonlinear optical properties of a material are fundamentally governed by its crystal symmetry,^[19,106–108] which in turn influences the SPDC process and the quantum states

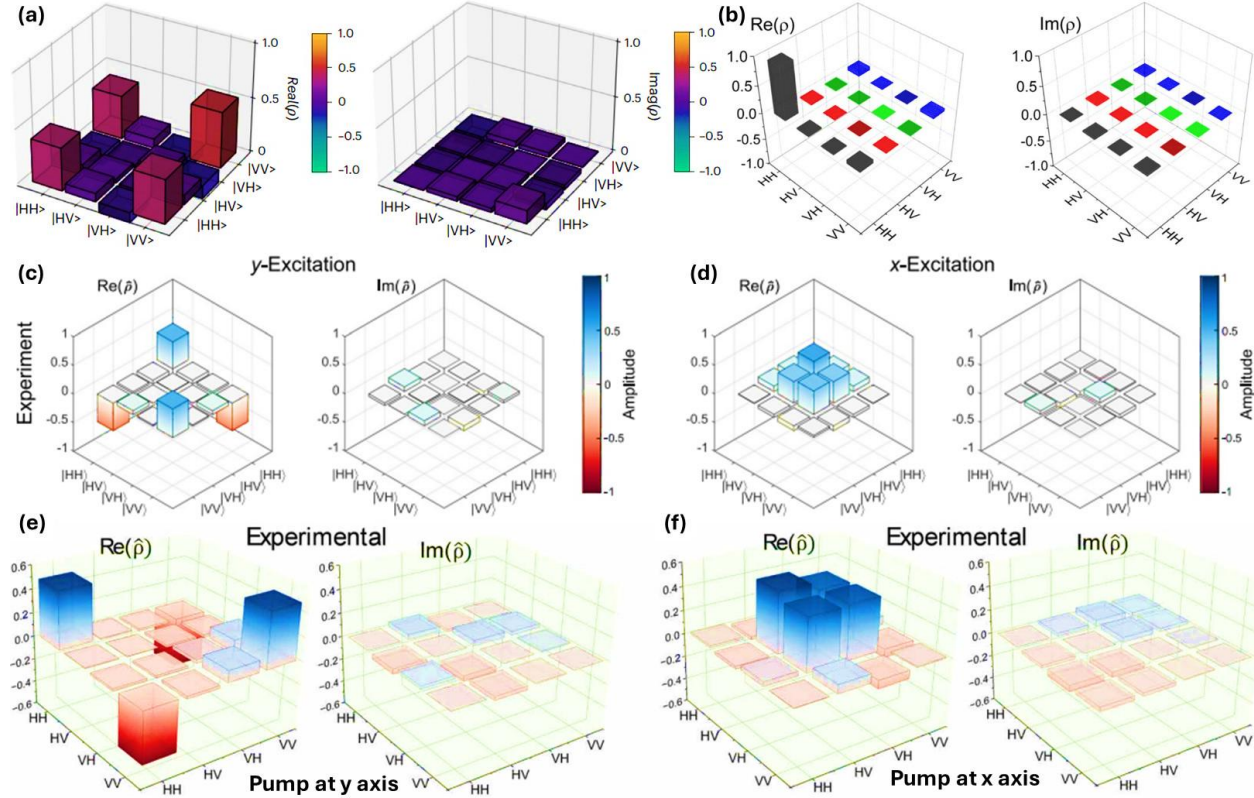


Figure 6 | Entangled quantum states. **a**, Quantum state tomography of the entangled photon pairs. *Left*: real part; *right*: imaginary part of the reconstructed density matrix. Reproduced with permission from.^[65] Copyright 2024, Springer Nature. **b**, Polarization dependent quantum state tomography in a single flake. Density matrices correspond to a fixed pump polarization of 45°. Adapted from Guo et al.^[23] Copyright 2024, Springer Nature. **c**, Polarization density matrices for *y*-polarized pump; **d**, for *x*-polarized pump. The real and imaginary parts are denoted by $\text{Re}(\rho)$ and $\text{Im}(\rho)$, respectively. The results obtained under *x*- and *y*- polarized excitation of 3R-MoS₂. Adapted from et al.^[23] Copyright 2024, Springer Nature. **e**, Density matrix of the generated photon quantum state under a pump polarization angle of 90°, corresponding to the entangled state $|\Psi\rangle =$

$\frac{1}{\sqrt{2}}(|\text{HH}\rangle - |\text{VV}\rangle)$, **d**, under a pump polarization angle of 0° , corresponding to $|\Psi\rangle = \frac{1}{\sqrt{2}}(|\text{HH}\rangle + |\text{VV}\rangle)$. Reproduced from Liang et al.,^[17] Copyright License 4.0 (CC BY- NC) 2025, AAAS.

of the generated EPPs. Experimental quantum state tomography of a vdW 3R-MoS₂ crystal has been reported, with the polarization resolved density matrices for *x*- and *y*- polarized excitation shown in **Figure 6c** and **6d**, respectively. Under *y*-polarized excitation, the generated quantum state exhibits a high fidelity of 0.96 with the maximally entangled Bell state $|\Psi\rangle = \frac{1}{\sqrt{2}}(|\text{HH}\rangle - |\text{VV}\rangle)$. For *x*-polarized excitation, the fidelity is slightly lower, at 0.84, corresponding to the state $|\Psi\rangle = \frac{1}{\sqrt{2}}(|\text{HH}\rangle + |\text{VV}\rangle)$. Additionally, the measured concurrences *C* are 0.973 ± 0.002 for *x*-polarization and 0.82 ± 0.02 for *y*-polarization.^[23] Such high concurrence values confirm the presence of strong quantum correlations between the photon pairs. Particularly, a concurrence value approaching unity signifies a high degree of entanglement between two qubits.

The polarization quantum state of *C*3 symmetric r-BN has been explored to produce entanglement between signal and idler photons.^[17] Quantum state tomography performed with a pump polarization angle of 90° reveals an entangled state described by $|\Psi\rangle = \frac{1}{\sqrt{2}}(|\text{HH}\rangle - |\text{VV}\rangle)$ with the corresponding density matrix shown in **Figure 6e**. In contrast, when the pump polarization is set to 0° , the generated state is $|\Psi\rangle = \frac{1}{\sqrt{2}}(|\text{HH}\rangle + |\text{VV}\rangle)$ as depicted in **Figure 6f**. The obtained fidelities for these states are 0.97 ± 0.013 and 0.933 ± 0.002 for the 90° and 0° pump polarizations, respectively. These high fidelity values promise that the prepared quantum states in r-BN are in excellent agreement with the ideal Bell states. Additionally, the strong entanglement quality is

Table 2. *Entangled photon pairs generated signals in vdW materials and their physical parameters. CAR is Coincidence to accidental ratio.*

Materia	Polarization	Photon pair	Fidelity	CAR	Ref
ls	Tomography Type	generation rate			
r-BN	-	8667 Hz/(mW·mm)	94%	2700	[97]
r-BN	2-photon	120 Hz	0.93	>200	[17]
NbOCl ₂	2-photon	31 kHz (mW·mm)	86%	1500	[65]
SiC	-	-	0.97	-	[109]
MoS ₂	2-photon	1563	0.96	0.973	[64]

confirmed by the high concurrence values of the photon pairs. A summary of the most recent quantum state tomography results for entangled photon pairs in various vdW materials is presented in **Table 2**. In addition, the crystal symmetry of vdW materials plays a crucial role in influencing the EPP generation rate. **Figure 7a** illustrates the EPP generation rates for various 2D vdW materials. Notably, r-BN exhibits an exceptionally high EPP generation rate compared to other layered materials. The combination of outstanding quantum tomographic performance and high EPP generation rates underscores the strong potential of these materials for next generation, practical on-chip quantum technologies.

5. On-chip quantum device applications

On-chip quantum technologies are leading the advancement of industrial quantum applications.^[3,33,34,110,111] In particular, integrated quantum photonics offers a compact, reliable,

reprogrammable, and scalable platform for both the exploration of fundamental quantum physics and the development of advanced quantum technologies. While bulk nonlinear crystals have been explored for on-chip device applications especially nonlinear photonic devices, vdW materials are now being considered as promising candidates for on-chip nonlinear photonic devices tailored for quantum applications. One key challenge lies in integrating SHG into existing silicon photonics platforms, primarily due to the lack of CMOS compatibility with conventional nonlinear materials. Additionally, the fixed and nontunable response of current nonlinear optical (NLO) materials significantly limits their practical implementation. Nonetheless, EPP based on vdW materials have yet to be explored for on-chip quantum device integration. However, the advances in on-chip nonlinear optics have been significantly propelled by the integration of 2D materials exhibiting

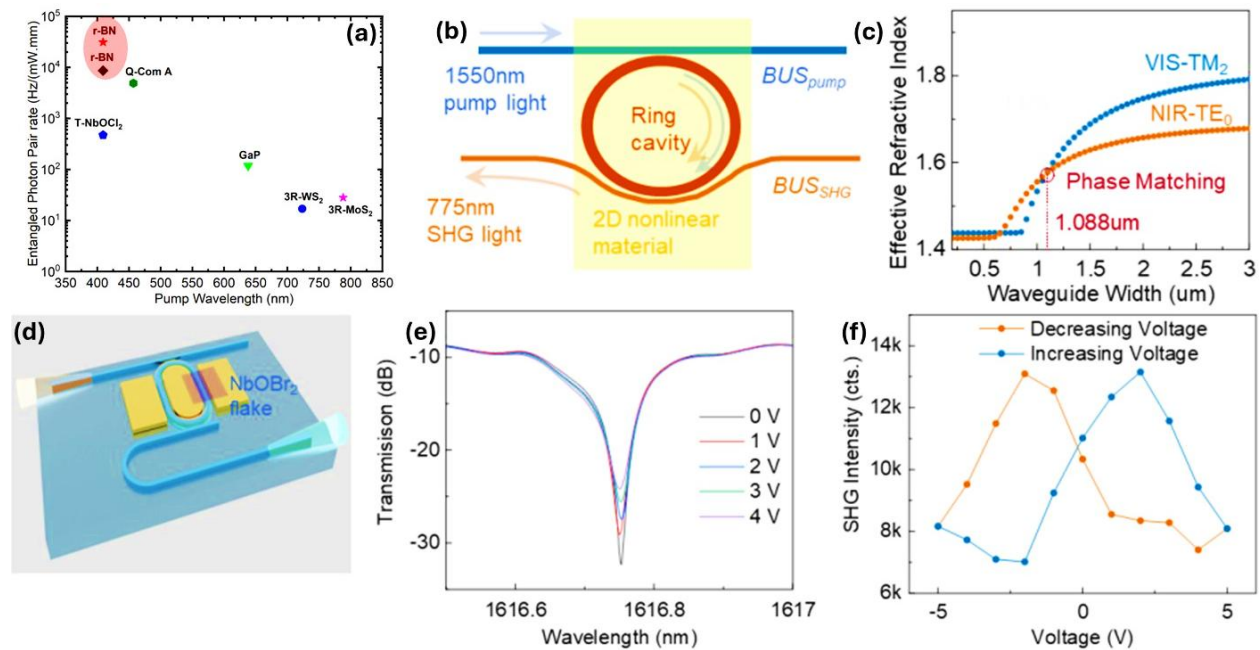


Figure 7. *a*, A comparison of entangled photon pair generation rates in various vdW materials.^[37,64,65,97,112,113] Among them, r-BN exhibited an excellent entangled photon pair generation rate. *b*, Schematic of on-chip SHG device. *c*, Refractive index of the SiN waveguide and the phase matching curve, *d*, Proposed tunable SHG device, *e*, Applied voltage dependent

device transmission spectra, f , Cyclic applied voltage dependent SHG intensity of the device. Adopted with permission from authors.^[110] Copyright SPIE, 2025.

strong second-order nonlinearities. A notable development is the use of niobium oxide dibromide (NbOBr_2) in silicon photonics platforms, as demonstrated by Gong et al.,^[110] where the material's intrinsic centrosymmetry breaking structure and in-plane ferroelectricity enable efficient and tunable SHG. Unlike traditional TMDs and layered materials whose SHG responses are layer dependent, NbOBr_2 offers robust, layer number independent SHG due to its anisotropic lattice distortions. When integrated into a SiN microring resonator, NbOBr_2 facilitates high efficiency SHG under low power continuous wave excitation, aided by cavity enhanced field confinement. More critically, the authors exploit the ferroelectric domain switching of NbOBr_2 to achieve nonvolatile electrical tuning of the SHG response, a novel mechanism that introduces hysteresis and memory effects into integrated nonlinear photonic devices (**Figure 7**). This multifunctional approach merges frequency conversion with programmable optical modulation, presenting a promising route toward compact, reconfigurable photonic circuits and next-generation light based quantum computing technologies.

6. Summary & Outlook

The review article outlines the fundamental properties of EPP generation, their characterization, and the purity of entangled photons in 2D vdW materials. It summarizes the nonlinear quantum optical properties of various 2D vdW materials and highlights the influence of crystallographic structures, especially crystal symmetry, on these properties. The NLO behavior of 2D vdW

materials, which underpins the SPDC process for generating EPPs, is explored in detail. Different crystallographic symmetries in layered materials reveal a wide range of second order nonlinear responses. For example, r-BN and 3R-MoS₂ exhibit rich nonlinear responses, enabling the generation of quantum EPPs via SPDC. Strong quantum correlations between EPPs have been confirmed through quantum state tomography. A high degree of entanglement between qubits is evident in the coincidence measurements performed on vdW materials. However, the realization of qubits with long coherence times and reduced noise remains largely unexplored. Nevertheless, experimental research on entangled photon generation in atomically thin layers and their on-chip integration for future quantum applications is still in its very early stages.

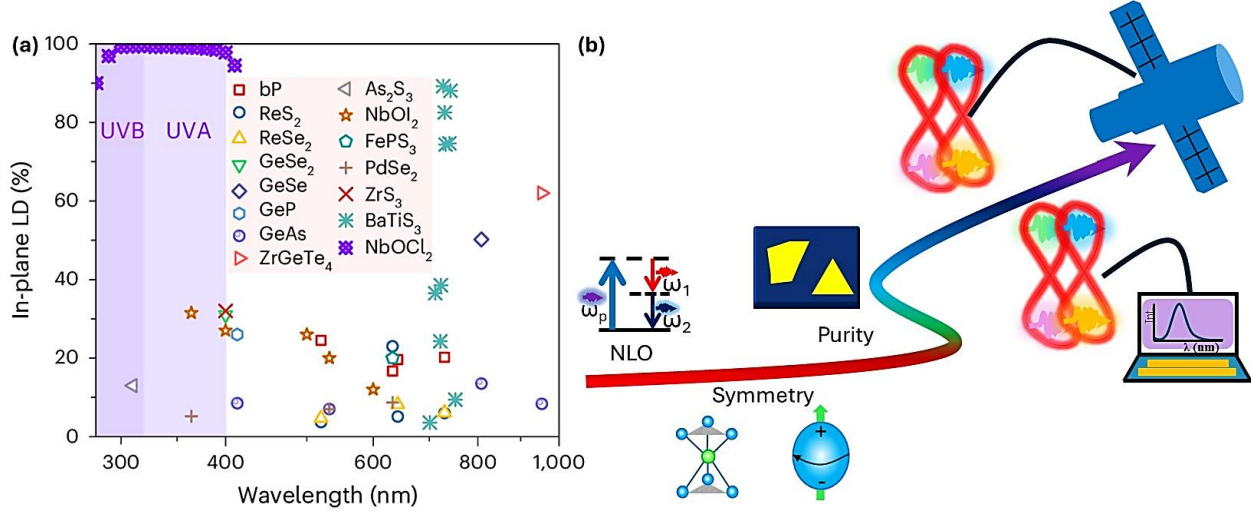


Figure 8. *a*, In-plane linear dichroism in recently developed vdW materials. Adopted with permission from.^[114] Copyright 2024, Springer Nature. and *b*, Schematic illustration of EPPs generations in vdW materials for future quantum photonic and quantum opto-electronic applications.

The generation of EPPs in nonlinear materials is reshaping the future of present quantum technology. Recent advancements are no longer confined to conventional, widely used nonlinear

bulk crystals but are progressively shifting towards quantum confined vdW materials.^[115] The boosting of classical and quantum nonlinear processes in layered vdW materials have emerged at the forefront of current research.^[25,105,116,117] Starting from layered graphene, the field now includes transition metal mono-, di-, and tri-chalcogenides, perovskites, metal-organic frameworks (MOFs), and singlecrystal molecular systems all of which exhibit remarkable nonlinear and quantum optical properties.^[95,118–126] Several of these materials have demonstrated exceptionally high second order ($\chi^{(2)}$) and higher order ($\chi^{(n)}$, $n \geq 3$) nonlinear coefficients.^[19,43,127–129] TMDs, in particular, have shown promising capabilities in producing EPPs with excellent associated parameters. Moreover, in-plane anisotropic layered materials exhibit the lowest crystal symmetry among known layered structures (**Figure 8**). Materials such as black phosphorene and monochalcogenides including SnS, SnSe, GeS, and GeSe possess rich anisotropic nonlinear coefficients.^[72,122,130–132] Additionally, two-dimensional phase change materials may hold the potential to revolutionize entangled photon pair generation due to their extraordinary second order nonlinear susceptibility.^[133–135] Beyond this, high dimensional quantum frequency combs^[136] in 2D vdW materials remain largely unexplored, potentially opening new avenues for quantum optics generation and device applications.

From a materials perspective, the application of 2D vdW materials in quantum entanglement and thus in quantum optics for on-chip quantum applications requires the growth of wafer scale, high crystal quality materials. Achieving high quality crystal growth presents challenges, as crystallinity and defects in thin layer 2D materials are critical issues. Although, the growth of specific crystal phases of atomically thin materials on appropriate substrates is a key focus area demanding substantial effort. In this context, more scalable and reliable synthesis methods capable of fabricating vdW materials and heterostructures with nanometric precision are

urgently needed for on-chip quantum device applications. Moreover, the discovery of EPPs in novel materials, such as magnetic 2D materials including anisotropic ones, remains largely unexplored.^[137–139] In addition, vdW heterostructures (HS), including those with mixed dimensionalities and crystal symmetries, can reduce PL induced background noise and hence can enhance the second order nonlinear susceptibility $\chi^{(2)}$, thereby improving SPDC and the generation of entangled photon pairs.

Finally, while challenges remain, the outlook for vdW materials in entangled photon generation is overwhelmingly positive. Their unique crystal symmetries, structures, and nonlinear properties, combined with cutting edge innovations, position them as transformative building blocks for the next generation of quantum technologies. Nonetheless, the generation of EPPs in ultrathin layered vdW materials is expected to enable advancements in quantum communication, quantum computing, quantum sensing for biological sciences, the semiconductor industry, and on-chip consumer applications.

Acknowledgements. The author is thankful for the kind permission from the corresponding publishers or authors to reproduce the figures included in this article.

Conflict of Interest. The authors declare no conflict of interest.

References

- [1] J. Wang, F. Sciarrino, A. Laing, M. G. Thompson, *Nat. Photon.* **2020**, *14*, 273.

- [2] E. Pelucchi, G. Fagas, I. Aharonovich, D. Englund, E. Figueroa, Q. Gong, H. Hannes, J. Liu, C. Y. Lu, N. Matsuda, J. W. Pan, F. Schreck, F. Sciarrino, C. Silberhorn, J. Wang, K. D. Jöns, *Nat. Rev. Phys.* **2022**, *4*, 194.
- [3] H. Mahmudlu, R. Johanning, A. van Rees, A. Khodadad Kashi, J. P. Epping, R. Haldar, K.-J. Boller, M. Kues, *Nat. Photon.* **2023**, *17*, 518.
- [4] *Nat. Rev. Phys.* **2025**, *7*.
- [5] P. Team, *Nature* **2025**.
- [6] V. Scarani, H. Bechmann-Pasquinucci, N. J. Cerf, M. Dušek, N. Lütkenhaus, M. Peev, *Rev. Mod. Phys.* **2009**, *81*, 1301.
- [7] H.-K. Lo, M. Curty, K. Tamaki, *Nat. Photon.* **2014**, *8*, 595.
- [8] Y. Adachi, T. Yamamoto, M. Koashi, N. Imoto, *Phys. Rev. Lett.* **2007**, *99*, 180503.
- [9] N. Gisin, R. Thew, *Nat. Photon.* **2007**, *1*, 165.
- [10] C. L. Degen, F. Reinhard, P. Cappellaro, *Rev. Mod. Phys.* **2017**, *89*.
- [11] A. Valencia, G. Scarcelli, Y. Shih, *Appl. Phys. Lett.* **2004**, *85*, 2655.
- [12] G. B. Lemos, V. Borish, G. D. Cole, S. Ramelow, R. Lapkiewicz, A. Zeilinger, *Nature* **2014**, *512*, 409.
- [13] D. Main, P. Drmota, D. P. Nadlinger, E. M. Ainley, A. Agrawal, B. C. Nichol, R. Srinivas, G. Araneda, D. M. Lucas, *Nature* **2025**, *638*, 383.
- [14] X. Chen, X. Lu, S. Dubey, Q. Yao, S. Liu, X. Wang, Q. Xiong, L. Zhang, A. Srivastava, *Nat. Phys.* **2019**, *15*, 221.

- [15] V. Sultanov, A. Kavčič, E. Kokkinakis, N. Sebastián, M. V. Chekhova, M. Humar, *Nature* **2024**, *631*, 294.
- [16] A. Rahmouni, R. Wang, J. Li, X. Tang, T. Gerrits, O. Slattery, Q. Li, L. Ma, *Light Sci. Appl.* **2024**, *13*, 110.
- [17] H. Liang, T. Gu, Y. Lou, C. Yang, C. Ma, J. Qi, A. A. Bettoli, X. Wang, *Sci. Adv.* **2025**, *11*, eadt3710.
- [18] W. Chen, S. Zhu, R. Duan, C. Wang, F. Wang, Y. Wu, M. Dai, J. Cui, S. H. Chae, Z. Li, X. Ma, Q. Wang, Z. Liu, Q. J. Wang, *Adv. Mater.* **2024**, *36*, 2400858.
- [19] Zhixiang Xie, Tianxiang Zhao, Xuechao Yu, Junjia Wang, *Small* **2024**, *20*, 2311621.
- [20] W. Huang, Y. Xiao, F. Xia, X. Chen, T. Zhai, *Adv. Funct. Mater.* **2024**, *34*, 2310726.
- [21] Y. Wang, K. D. Jöns, Z. Sun, *Appl. Phys. Rev.* **2021**, *8*, 011314.
- [22] C. Trovatello, A. Marini, M. Cotrufo, A. Alù, P. J. Schuck, G. Cerullo, *ACS Photonics* **2024**, *11*, 2860.
- [23] Q. Guo, Y.-K. Wu, D. Zhang, Q. Zhang, G.-C. Guo, A. Alù, X.-F. Ren, C.-W. Qiu, *Nat. Commun.* **2024**, *15*, 10461.
- [24] C. Okoth, A. Cavanna, T. Santiago-Cruz, M. V. Chekhova, *Phys. Rev. Lett.* **2019**, *123*, 263602.
- [25] L. Gu, Y. Zhou, *Appl. Phys. Rev.* **2025**, *12*, 011335.
- [26] J. Kang, L. Zhou, Y. Wang, J. Zhang, Q. Long, X. Zhong, X. Li, Y. Wang, S. Xiao, J. He, *J. Phys. Chem. Lett.* **2025**, 4262.

- [27] L. Ye, W. Zhou, D. Huang, X. Jiang, Q. Guo, X. Cao, S. Yan, X. Wang, D. Jia, D. Jiang, Y. Wang, X. Wu, X. Zhang, Y. Li, H. Lei, H. Gou, B. Huang, *Nat. Commun.* **2023**, *14*, 5911.
- [28] Q. Guo, X. Z. Qi, L. Zhang, M. Gao, S. Hu, W. Zhou, W. Zang, X. Zhao, J. Wang, B. Yan, M. Xu, Y. K. Wu, G. Eda, Z. Xiao, S. A. Yang, H. Gou, Y. P. Feng, G. C. Guo, W. Zhou, X. F. Ren, C. W. Qiu, S. J. Pennycook, A. T. S. Wee, *Nature* **2023**, *613*, 53.
- [29] Z. Li, S. Wang, C. Wang, X. Zhang, Z. Yu, S. Du, Z. Zeng, Y. Dai, Y. Zhang, X. Liu, J. Sun, J. Xue, Z. Wu, L. Fan, J. Dai, K. Zhai, A. Nie, Z. Liu, Y. Cheng, *Small* **2024**, *21*, 2407729.
- [30] Y. Ding, A. Huang, Yu Wu, L. Zhou, *Appl. Phys. Lett.* **2024**, *125*, 151902.
- [31] C. Trovatello, A. Marini, X. Xu, C. Lee, F. Liu, N. Curreli, C. Manzoni, S. Dal Conte, K. Yao, A. Ciattoni, J. Hone, X. Zhu, P. J. Schuck, G. Cerullo, *Nat. Photon.* **2021**, *15*, 6.
- [32] M. C. Lemme, D. Akinwande, C. Huyghebaert, C. Stampfer, *Nat. Commun.* **2022**, *13*, 1392.
- [33] H. Tang, Y. Wang, X. Ni, K. Watanabe, T. Taniguchi, P. Jarillo-Herrero, S. Fan, E. Mazur, A. Yacoby, Y. Cao, *Nature* **2024**, *632*, 1038.
- [34] C. Frydendahl, T. Yezekyan, V. A. Zenin, S. I. Bozhevolnyi, *Nano Lett.* **2025**, *25*, 6414.
- [35] Y. Zhang, J. Wu, J. Hu, L. Jia, D. Jin, B. Jia, X. Hu, D. J. Moss, Q. Gong, *APL Photonics* **2025**, *10*, 040903.
- [36] A. R. P. Montblanch, M. Barbone, I. Aharonovich, M. Atatüre, A. C. Ferrari, *Nat. Nanotechnol.* **2023**, *18*, 555.
- [37] J. Feng, Y.-K. Wu, R. Duan, J. Wang, W. Chen, J. Qin, Z. Liu, G.-C. Guo, X.-F. Ren, C.-W. Qiu, *eLight* **2024**, *4*, 16.

- [38] G. Zograf, A. Yu. Polyakov, M. Bancerek, T. J. Antosiewicz, B. Küçüköz, T. O. Shegai, *Nat. Photon.* **2024**, *18*, 751.
- [39] R. C. Eckardt, H. Masuda, Y. X. Fan, R. L. Byer, *IEEE J. Quantum Electron.* **1990**, *26*, 922.
- [40] I. Shoji, T. Kondo, A. Kitamoto, M. Shirane, R. Ito, *J. Opt. Soc. Am. B* **1997**, *14*, 2268.
- [41] C. Trovatello, C. Ferrante, B. Yang, J. Bajo, B. Braun, Z. H. Peng, X. Xu, P. K. Jenke, A. Ye, M. Delor, D. N. Basov, J. Park, P. Walther, C. R. Dean, L. A. Rozema, A. Marini, G. Cerullo, P. J. Schuck, *Nat. Photon.* **2025**, *19*, 291.
- [42] H. Hong, C. Huang, C. Ma, J. Qi, X. Shi, C. Liu, S. Wu, Z. Sun, E. Wang, K. Liu, *Phys. Rev. Lett.* **2023**, *131*, 233801.
- [43] J. Qi, C. Ma, Q. Guo, C. Ma, Z. Zhang, F. Liu, X. Shi, L. Wang, M. Xue, M. Wu, P. Gao, H. Hong, X. Wang, E. Wang, C. Liu, K. Liu, *Adv. Mater.* **2024**, *36*, 2303122.
- [44] H. Park, N. Park, J. Lee, *Nano Lett.* **2025**, *24*, 13192.
- [45] G. P. Martins, O. L. Berman, G. Gumbs, Y. E. Lozovik, *Phys. Rev. B* **2022**, *106*, 104304.
- [46] G. P. Martins, O. L. Berman, G. Gumbs, Y. E. Lozovik, *Phys. Rev. B* **2025**, *111*, 45425.
- [47] L. Chen, Z. Li, Q. Li, Q. Zheng, J. Zhao, *Adv. Opt. Mater.* **2025**, *13*, 2403069.
- [48] S. Son, Y. Lee, J. H. Kim, B. H. Kim, C. Kim, W. Na, H. Ju, S. Park, A. Nag, K. J. Zhou, Y. W. Son, H. Kim, W. S. Noh, J. H. Park, J. S. Lee, H. Cheong, J. H. Kim, J. G. Park, *Adv. Mater.* **2022**, *34*, 2109144.
- [49] D. Lachance-Quirion, S. P. Wolski, Y. Tabuchi, S. Kono, K. Usami, Y. Nakamura, *Science (1979)* **2020**, *367*, 425.

- [50] R. Lü, H. Zhan, D. Kong, F. Wang, *Opt. Lett.* **2024**, *49*, 7032.
- [51] N. Benrass, A. Hidki, D. Aoune, N. Habiballah, *Russ. Phys.* **2024**, *67*, 829.
- [52] M. Amazioug, B. Teklu, M. Asjad, *Sci. Rep.* **2023**, *13*, 3833.
- [53] T. Zhang, S. Murakami, *Phys. Rev. B* **2022**, *105*, 235204.
- [54] X. Xi, J. Ma, X. Sun, *Adv. Mater* **2025**, *37*, 2309015.
- [55] J. D. Mella, H. L. Calvo, L. E. F. Foa Torres, *Nano Lett.* **2023**, *23*, 11013.
- [56] D. Buterakos, S. Das Sarma, *PRX Quantum* **2021**, *2*, 40358.
- [57] H. S. Borges, C. A. N. Júnior, D. S. Brandão, F. Liu, V. V. R. Pereira, S. J. Xie, F. Qu, A. M. Alcalde, *Phys. Rev. B* **2023**, *107*, 35404.
- [58] N. Stefanidis, I. S. Villadiego, *Phys. Rev. B* **2023**, *108*, 235137.
- [59] M. A. Selim, M. Ehrhardt, Y. Ding, H. M. Dinani, Q. Zhong, A. Perez-Leija, Ş. K. Özdemir, M. Heinrich, A. Szameit, D. N. Christodoulides, M. Khajavikhan, *Science (1979)* **2025**, 387, 1424.
- [60] X. You, Y. Li, *Phys. Rev. A* **2019**, *100*, 053842.
- [61] C. Zhang, Y. F. Huang, B. H. Liu, C. F. Li, G. C. Guo, *Adv. Quantum Technol.* **2021**, *4*, 2000132.
- [62] K. S. Novoselov, A. K. Geim, S. V. Morozov, D. Jiang, Y. Zhang, S. V. Dubonos, I. V. Grigorieva, A. A. Firsov, *Science (1979)* **2004**, *306*, 666.
- [63] Y. M. He, G. Clark, J. R. Schaibley, Y. He, M. C. Chen, Y. J. Wei, X. Ding, Q. Zhang, W. Yao, X. Xu, C. Y. Lu, J. W. Pan, *Nat. Nanotechnol.* **2015**, *10*, 497.

- [64] M. A. Weissflog, A. Fedotova, Y. Tang, E. A. Santos, B. Laudert, S. Shinde, F. Abtahi, M. Afsharnia, I. Pérez Pérez, S. Ritter, H. Qin, J. Janousek, S. Shradha, I. Staude, S. Saravi, T. Pertsch, F. Setzpfandt, Y. Lu, F. Eilenberger, *Nat. Commun.* **2024**, *15*, 7600.
- [65] L. Kallioniemi, X. Lyu, R. He, A. Rasmita, R. Duan, Z. Liu, W. Gao, *Nat. Photon.* **2025**, *19*, 142.
- [66] Y. Li, Y. Rao, K. F. Mak, Y. You, S. Wang, C. R. Dean, T. F. Heinz, *Nano Lett.* **2013**, *13*, 3329.
- [67] M. Zhao, Z. Ye, R. Suzuki, Y. Ye, H. Y. Zhu, J. Xiao, Y. Wang, Y. Iwasa, X. Zhang, *Light Sci. Appl.* **2016**, *5*, e16131.
- [68] J.-D. Zheng, Y.-K. Zhang, W.-Y. Tong, Y.-H. Shen, Y.-F. Zhao, Y.-F. Tan, J.-H. Chu, C.-G. Duan, *ACS Appl. Electron Mater.* **2024**, *6*, 2059.
- [69] A. S. Sarkar, E. Stratakis, *Adv. Sci.* **2020**, *7*, 1.
- [70] A. S. Sarkar, I. Konidakis, E. Gagaoudakis, G. M. Maragkakis, S. Psilodimitrakopoulos, D. Katerinopoulou, L. Sygellou, G. Deligeorgis, V. Binas, I. M. Oikonomou, P. Komninou, G. Kiriakidis, G. Kioseoglou, E. Stratakis, *Adv. Sci.* **2023**, *10*, 2201842.
- [71] L. Li, W. Han, L. Pi, P. Niu, J. Han, C. Wang, B. Su, H. Li, J. Xiong, Y. Bando, T. Zhai, *Info Mat.* **2019**, *1*, 54.
- [72] A. S. Sarkar, A. Mushtaq, D. Kushavah, S. K. Pal, *npj 2D Mater. Appl.* **2020**, *4*, 1.
- [73] M. Zhu, M. Zhong, X. Guo, Y. Wang, Z. Chen, H. Huang, J. He, C. Su, K. P. Loh, *Adv. Opt. Mater.* **2021**, *9*, 2101200.

- [74] G. M. Maragkakis, S. Psilodimitrakopoulos, L. Mouchliadis, A. S. Sarkar, A. Lemonis, G. Kioseoglou, E. Stratakis, *Adv. Opt. Mater.* **2022**, *10*, 2102776.
- [75] R. Moqbel, R. Nanae, S. Kitamura, M. Lee, Y. Lan, C. Lee, K. Nagashio, K. Lin, *Adv. Opt. Mater.* **2024**, *12*, 2400355.
- [76] C. Gong, L. Li, Z. Li, H. Ji, A. Stern, Y. Xia, T. Cao, W. Bao, C. Wang, Y. Wang, Z. Q. Qiu, R. J. Cava, S. G. Louie, J. Xia, X. Zhang, *Nature* **2017**, *546*, 265.
- [77] Z. Sun, Y. Yi, T. Song, G. Clark, B. Huang, Y. Shan, S. Wu, D. Huang, C. Gao, Z. Chen, M. McGuire, T. Cao, D. Xiao, W. T. Liu, W. Yao, X. Xu, S. Wu, *Nature* **2019**, *572*, 497.
- [78] H. Chu, C. J. Roh, J. O. Island, C. Li, S. Lee, J. Chen, J. G. Park, A. F. Young, J. S. Lee, D. Hsieh, *Phys. Rev. Lett.* **2020**, *124*, 027601.
- [79] K. Lee, A. H. Dismukes, E. J. Telford, R. A. Wiscons, J. Wang, X. Xu, C. Nuckolls, C. R. Dean, X. Roy, X. Zhu, *Nano Lett.* **2021**, *21*, 3511.
- [80] D. Wu, Y. Xu, M. Ye4, W. Duan, *Sci. Adv.* **2025**, *11*, eadu6562.
- [81] Z. Ni, N. Huang, A. V. Haglund, D. G. Mandrus, L. Wu, *Nano Lett.* **2022**, *22*, 3283.
- [82] Dezhao Wu, Meng Ye, Haowei Chen, Yong Xu, *npj Comput. Mater.* **2024**, *10*, 79.
- [83] A. Kirilyuk, T. Rasing, *J. Opt. Soc. Am. B* **2005**, *22*, 148.
- [84] M. Fiebig, V. V. Pavlov, R. V. Pisarev, *J. Opt. Soc. Am. B* **2005**, *22*.
- [85] N. Kumar, S. Najmaei, Q. Cui, F. Ceballos, P. M. Ajayan, J. Lou, H. Zhao, *Phys. Rev. B* **2013**, *87*, 161403.

- [86] H. Chen, V. Corboliou, A. S. Solntsev, D. Y. Choi, M. A. Vincenti, D. de Ceglia, C. de Angelis, Y. Lu, D. N. Neshev, *Light Sci. Appl.* **2017**, *6*, e17060.
- [87] A. Autere, H. Jussila, A. Marini, J. R. M. Saavedra, Y. Dai, A. Säynätjoki, L. Karvonen, H. Yang, B. Amirsolaimani, R. A. Norwood, N. Peyghambarian, H. Lipsanen, K. Kieu, F. J. G. De Abajo, Z. Sun, *Phys. Rev. B* **2018**, *98*, 115426.
- [88] C. Janisch, Y. Wang, D. Ma, N. Mehta, A. L. Elías, N. Perea-López, M. Terrones, V. Crespi, Z. Liu, *Sci. Rep.* **2014**, *4*, 5530.
- [89] J. Ribeiro-Soares, C. Janisch, Z. Liu, A. L. Elías, M. S. Dresselhaus, M. Terrones, L. G. Cançado, A. Jorio, *2D Mater.* **2015**, *2*, 045015.
- [90] S. Kim, J. E. Fröch, A. Gardner, C. Li, I. Aharonovich, A. S. Solntsev, *Opt. Lett.* **2019**, *44*, 5792.
- [91] C. J. Kim, L. Brown, M. W. Graham, R. Hovden, R. W. Havener, P. L. McEuen, D. A. Muller, J. Park, *Nano Lett.* **2013**, *13*, 5660.
- [92] K. Younus, Y. Zhou, M. Zhu, D. Xu, X. Guo, A. Ahmed, F. Ouyang, H. Huang, S. Xiao, Z. Chen, J. He, *J. Phys. Chem. Lett.* **2024**, *15*, 4992.
- [93] I. Abdelwahab, B. Tilmann, Y. Wu, D. Giovanni, I. Verzhbitskiy, M. Zhu, R. Berté, F. Xuan, L. de S. Menezes, G. Eda, T. C. Sum, S. Y. Quek, S. A. Maier, K. P. Loh, *Nat. Photon.* **2022**, *16*, 644.
- [94] C. Yuan, X. Li, S. Semin, Y. Feng, T. Rasing, J. Xu, *Nano Lett.* **2018**, *18*, 5411.
- [95] M. Zhu, D. Xu, Y. Ouyang, H. Zhang, L. Liu, J. Meng, S. Xiao, Z. Chen, J. He, *J. Phys. Chem. Lett.* **2024**, *15*, 12120.

- [96] S. E. Harris, M. K. Oshman, R. L. Byer, *Phys. Rev. Lett.* **1967**, *18*, DOI 10.1103/PhysRevLett.18.732.
- [97] X. Lyu, L. Kallioniemi, H. Hong, R. Qu, Y. Zhang, J. Zúñiga-Perez, K. Liu, W. Gao, *Nat. Commun.* **2025**, *16*, 1899.
- [98] Y. Tang, K. Sripathy, H. Qin, Z. Lu, G. Guccione, J. Janousek, Y. Zhu, M. M. Hasan, Y. Iwasa, P. K. Lam, Y. Lu, *Nat. Commun.* **2024**, *15*, 9979.
- [99] M. Cramer, M. B. Plenio, S. T. Flammia, R. Somma, D. Gross, S. D. Bartlett, O. Landon-Cardinal, D. Poulin, Y.-K. Liu, *Nat. Commun.* **2010**, *1*, 149.
- [100] J. Zhang, S. S. Hegde, D. Suter, *Phys. Rev. Lett.* **2023**, *130*, 90801.
- [101] M. Steffen, M. Ansmann, R. C. Bialczak, H. Katz, E. Lucero, R. McDermott, M. Neeley, E. M. Weig, A. N. Cleland, J. M. Martinis, *Science (1979)* **2006**, *313*, 1423.
- [102] E. A. Wollack, A. Y. Cleland, R. G. Gruenke, Z. Wang, P. Arrangoiz-Arriola, A. H. Safavi-Naeini, *Nature* **2022**, *604*, 463.
- [103] D. F. V. James, P. G. Kwiat, W. J. Munro, A. G. White, *Phys. Rev. A* **2001**, *64*, 052312.
- [104] W. K. Wootters, *Phys. Rev. Lett.* **1998**, *80*, 2245.
- [105] P. Laurell, A. Scheie, E. Dagotto, D. A. Tennant, *Adv. Quantum Technol.* **2025**, *8*, 2400196.
- [106] H. Wang, X. Qian, *Nano Lett.* **2017**, *17*, 5027.
- [107] Y. Shan, Y. Li, D. Huang, Q. Tong, W. Yao, W. T. Liu, S. Wu, *Sci. Adv.* **2018**, *4*, eaat0074.
- [108] C. Qian, S. Jiang, T. Wu, H. Weng, C. Yu, R. Lu, *Phys. Rev. B* **2024**, *109*, 205401.

- [109] P. V. Klimov, A. L. Falk, D. J. Christle, V. V. Dobrovitski, D. D. Awschalom, *Sci. Adv.* **2015**, *1*, e1501015.
- [110] X. Gong, R. Duan, T. X. Guo, W. Chen, Z. Liu, S. Chae, *Proc. SPIE* **2025**, *13368*, 133680A.
- [111] W. Luo, L. Cao, Y. Shi, L. Wan, H. Zhang, S. Li, G. Chen, Y. Li, S. Li, Y. Wang, S. Sun, M. F. Karim, H. Cai, L. C. Kwek, A. Q. Liu, *Light Sci. Appl.* **2023**, *12*, 175.
- [112] V. Sultanov, T. Santiago-Cruz, M. V. Chekhova, *Opt. Lett.* **2022**, *47*, DOI 10.1364/ol.458133.
- [113] T. Santiago-Cruz, S. D. Gennaro, O. Mitrofanov, S. Addamane, J. Reno, I. Brener, M. V. Chekhova, *Science (1979)* **2022**, *377*, 991.
- [114] Q. Guo, Q. Zhang, T. Zhang, J. Zhou, S. Xiao, S. Wang, Y. Ping Feng, C.-W. Qiu, *Nat. Photon.* **2024**, *18*, 1170.
- [115] X. Liu, M. C. Hersam, *Nat. Rev. Mater.* **2019**, *4*, 669.
- [116] X. Lyu, L. Kallioniemi, H. Cai, L. An, R. Duan, S. J. Wu, Q. Tan, C. Zhang, R. He, Y. Miao, Z. Liu, A. Ling, J. Z. Perez, W. Gao, *ArXiv* **2025**.
- [117] M. Turunen, M. Brotons-Gisbert, Y. Dai, Y. Wang, E. Scerri, C. Bonato, K. D. Jöns, Z. Sun, B. D. Gerardot, *Nat. Rev. Phys.* **2022**, *4*, 219.
- [118] Z. Chen, G. Gallo, V. A. Sawant, T. Zhang, M. Zhu, L. Liang, A. Chanthapally, G. Bolla, H. S. Quah, X. Liu, K. P. Loh, R. E. Dinnebier, Q. H. Xu, J. J. Vittal, *Angew. Chem. Int. Ed.* **2020**, *59*, 833.
- [119] Z. Chen, Q. Zhang, M. Zhu, H. Chen, X. Wang, S. Xiao, K. P. Loh, G. Eda, J. Meng, J. He, *J. Phys. Chem. Lett.* **2021**, *12*, 7010.

- [120] Z. Wang, R. Shi, I. Tahir, D. P. Karothu, P. Cheng, W. Han, L. Li, Y. Zheng, P. Naumov, J. Xu, X.-H. Bu, *J. Am. Chem. Soc.* **2025**, *147*, 7749.
- [121] K. M. Holland, A. Alejandro, D. J. H. Ludlow, P. K. Petersen, M. A. Wright, C. C. Chartrand, D. J. Michaelis, J. A. Johnson, J. E. Patterson, *Opt. Lett.* **2023**, *48*, 5855.
- [122] F. Xia, H. Wang, J. C. M. Hwang, A. H. C. Neto, L. Yang, *Nat. Rev. Phys.* **2019**, *1*, 306.
- [123] D. J. Morrow, M. P. Hautzinger, D. P. Lafayette, J. M. Scheeler, L. Dang, M. Leng, D. D. Kohler, A. M. Wheaton, Y. Fu, I. A. Guzei, J. Tang, S. Jin, J. C. Wright, *J. Phys. Chem. Lett.* **2020**, *11*, 6551.
- [124] W. J. Wei, X. X. Jiang, L. Y. Dong, W. W. Liu, X. B. Han, Y. Qin, K. Li, W. Li, Z. S. Lin, X. H. Bu, P. X. Lu, *J. Am. Chem. Soc.* **2019**, *141*.
- [125] A. S. Sarkar, A. Kumari, Anchala, N. Nakka, R. Ray, E. Stratakis, S. K. Pal, *Appl. Phys. Lett.* **2021**, *119*, 241902.
- [126] A. Verma, A. Soni, A. S. Sarkar, S. K. Pal, *Opt. Lett.* **2023**, *48*, 4641.
- [127] S. Psilodimitrakopoulos, S. Ilin, L. E. Zelenkov, S. Makarov, Emmanuel. Stratakis, *Nanophotonics* **2024**, *13*, 3181.
- [128] L. Yue, C. Liu, S. Han, H. Hong, Y. Wang, Q. Liu, J. Qi, Y. Li, D. Wu, K. Liu, E. Wang, T. Dong, N. Wang, *Science (1979)* **2024**, *10*, eadn6216.
- [129] B. Li, H. Li, C. Wu, L. Fu, D. W. Boukhvalov, M. G. Humphrey, C. Zhang, Z. Huang, *Angew. Chem. Int. Ed.* **2024**, *63*, e202406941.
- [130] S. Barraza-Lopez, B. M. Fregoso, J. W. Villanova, S. S. P. Parkin, K. Chang, *Rev. Mod. Phys.* **2021**, *93*, 011001.

- [131] G. M. Maragkakis, S. Psilodimitrakopoulos, L. Mouchliadis, A. S. Sarkar, A. Lemonis, G. Kioseoglou, E. Stratakis, *Adv. Opt. Mater.* **2024**, *12*, 2401321.
- [132] M. B. P. Querne, J. M. Bracht, J. L. F. Da Silva, A. Janotti, M. P. Lima, *Phys. Rev. B* **2023**, *108*, 085409.
- [133] Z. Lou, Y. Zhao, Z. Gong, Z. Zhu, M. Wu, T. Wang, J. Wang, H. Qi, H. Zuo, Z. Xu, J. Shen, Z. Wang, L. Li, S. Xu, W. Kong, W. Li, X. Zheng, H. Wang, X. Lin, *Adv. Mater.* **2024**, *37*, 2409887.
- [134] Y. Zhao, J. Zhao, Y. Guo, J. Zhao, J. Feng, Y. Geng, J. Yang, H. Gao, M. Yuan, L. Jiang, Y. Wu, *SmartMat* **2022**, *3*, 657.
- [135] B. Li, W. Rao, X. You, P. Wang, J. Wei, Z. Wei, H. Zhang, H. Cai, *Inorg. Chem.* **2023**, *62*, 942.
- [136] K.-C. Chang, X. Cheng, M. C. Sarihan, C. W. Wong, *Newton* **2025**, *1*, 100024.
- [137] Z. da Gao, Z. hui yi Jiang, J. dong Li, B. wen Li, Y. yang Long, X. mei Li, J. Yin, W. lin Guo, *Adv. Eng. Mater.* **2022**, *24*, 2200519.
- [138] S. Chen, Z. Tang, M. Fang, R. Sun, X. Zhang, L. Xiao, S. S. Mohajerani, N. Liu, Y. Zhang, A. S. Sarkar, D. Sun, S. Strauf, E. H. Yang, *Adv. Funct. Mater.* **2025**, 2418647.
- [139] M. Gibertini, M. Koperski, A. F. Morpurgo, K. S. Novoselov, *Nat. Nanotechnol.* **2019**, *14*, 408.